

Influence of surface quantum effects on optical characteristics of a pair of plasmonic nanoparticles

© Yu.A. Eremin, V.V. Lopushenko

Moscow State University, Moscow, Russia

e-mail: lopushnk@cs.msu.ru

Received July 07, 2023

Revised September 04, 2023

Accepted September 06, 2023

The influence of quantum effects, such as spatial nonlocality and splitting of electron cloud near the surface, on the extinction cross-section and field intensity in the gap between particles was analyzed via the Discrete Source Method using a pair of plasmonic gold nanoparticles. In this case, spatial nonlocality is described within the framework of the Generalized Nonlocal Optical Response Theory, while the splitting of the electron cloud is accounted for by using the theory of mesoscopic boundary conditions with Feibelman parameters. It has been found that mesoscopic boundary conditions lead to restoring of the plasmon resonance amplitude compared to the volume nonlocal effect.

Keywords: Discrete Source Method, nonlocal effect, mesoscopic boundary conditions, Feibelman parameters.

DOI: 10.61011/EOS.2023.08.57294.5402-23

Introduction

Processes arising from the interaction of light with plasmonic metal nanostructures are of increasing interest to researchers and technologists because the discovered effects are widely used in various fields of science and technology, including physics, biology and healthcare. Plasmonic structures allow the manipulation of light at the nanoscale and make it possible to obtain strong, highly concentrated and localized electromagnetic fields. This is achieved through localized surface plasmon resonance (PR), a well-known phenomenon that occurs in metal nanostructures due to collective vibrations of free electrons under the effect of external electromagnetic field. Plasmon resonance leads to an increase in field intensity by several orders of magnitude at a certain frequency of the external excitation, which makes it possible not only to achieve a giant gain of the field near the structure but also to concentrate and retain it in volumes much greater than the Rayleigh limit. These properties of plasmonic nanostructures form the basis of numerous practical applications [1,2].

The interest in metal structures with nanogap characteristics is mainly due to their use in important applications in spectroscopy, associated, in particular, with experimental results obtained in the study of single-molecule surface-enhanced Raman scattering [3]. The maximum level of sensitivity achieved in such structures is determined precisely by the presence of localized surface plasmon resonance associated with the presence of a nanogap, inside which the increase in the electric field strength can be as high as several orders of magnitude [4]. An example of the implementation of such a plasmonic structure can be paired particles (dimers) of noble metals. They are formed in such a way as to minimize the gap between them. It

should be noted that modern synthesis technologies make it possible to obtain a subnanometer gap ~ 1 nm between nanoparticles [5]. Paired particles are used to decipher the spectra of individual molecules and implement biosensors with a wide range of practical applications [6–8].

A decrease in the size of particles of noble metals leads to the emergence of quantum effects in them, such as bulk nonlocality and the release of free electrons beyond the surface of the particles [9,10]. When studying paired nanoparticles, it is customary to distinguish three gap regimes depending on the size of the gap δ [11].

1. For $\delta \geq 2$ nm, classical Maxwell theory gives essentially the same results as the nonlocal response approximation.

2. For 2 nm $\geq \delta \geq 0.5$ nm, strong nonlocal effects appear, and both local and nonlocal descriptions predict the same qualitative behavior of optical characteristics, but significant quantitative differences arise both in the PR amplitude and its position in the frequency domain.

3. For $\delta \leq 0.5$ nm, the main role is played by quantum effects, such as the spill out of electrons outside the metal and the tunneling of electrons between nanoparticles [12].

It is important to note that in the case of paired particles, the use of purely quantum research methods, such as the time-dependent density functional theory (TDDFT) [13], seems ineffective due to the significant volume of the metal nanostructure, which requires enormous computing power and time [14]. Therefore, in this case, quasi-classical approaches have become more widespread. Among them, the hydrodynamic Drude theory and its generalization, the generalized nonlocal optical response (GNOR) theory [15,16], should be highlighted. This theory allows taking into account two bulk quantum effects: the appearance of longitudinal fields inside plasmonic nanoparticles

and the Landau damping. GNOR gives results that coincide with other theories and experiment [17], however, it does not take into account the spill out of electrons beyond the surface, which may be critical when analyzing the spectral characteristics of fields in the subnanometer gap of paired nanoparticles [18,19].

To take into account the surface quantum effect, surface response functions (SRF) — Feibelman parameters [20] have recently been developed. These parameters are included in the so-called „mesoscopic“ boundary conditions [21], which are a generalization of the classical conditions for coupling the fields at the interfaces of media with different characteristics, taking into account the occurrence of induced surface charges and currents, with the field inside the medium being described by classical Maxwell's equations. This approach is considered as the missing link connecting the purely quantum description of effects with the quasi-classical one [10,22].

This study, based on a modification of the Discrete Sources Method (DSM) [23,24], investigates the influence of quantum bulk and surface effects on the optical characteristics of a pair of two gold spheroidal nanoparticles, including the field intensity in the gap between them. Two models are considered in the study: the GNOR theory [16] and the theory with mesoscopic boundary conditions — SRF [22]. It should be reminded that DSM is a numerical-analytical method where fields in the vicinity of surfaces of the scattering structure are represented by analytical functions. Therefore, the presence of surface divergence in mesoscopic boundary conditions [22] does not pose any particular difficulties for the numerical implementation of a new DSM computational scheme.

Statement of the boundary problem of diffraction

We will consider the problem of diffraction of a plane P -polarized electromagnetic wave $\{\mathbf{E}_0, \mathbf{H}_0\}$ on a pair of identical axisymmetric homogeneous nanoparticles having a common axis of rotation (Fig. 1). As it is established in [23], the most noticeable PR occurs precisely in the case of P -polarization. Let us denote the internal regions of the particles as $D_{1,2}$, and denote the external region as D_e . The corresponding smooth particle surfaces will be denoted as $\partial D_{1,2} \in C^{(2,\tau)}$. Assume that all media are non-magnetic, and the time dependence is chosen in the form of $\exp(j\omega t)$.

When particle sizes are less than 20 nm, bulk nonlocality arises inside them [15], which leads to the emergence of longitudinal (irrotational) fields in addition to classical transverse (divergence-free) fields. Following the approach of [24], we will use the GNOR theory in this case.

Let us proceed to a description of the SRF theory and consider the mathematical formulation of the diffraction problem with mesoscopic boundary conditions.

In the external region, the scattered field $\{\mathbf{E}_e, \mathbf{H}_e\}$ satisfies the system of Maxwell's equations of the following

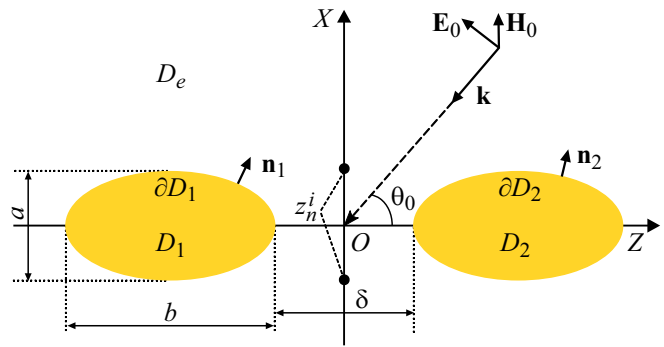


Figure 1. Geometry of the problem.

form

$$\text{rot}\mathbf{H}_e = jk\varepsilon_e\mathbf{E}_e; \quad \text{rot}\mathbf{E}_e = -jk\mathbf{H}_e; \quad \text{in } D_e. \quad (1)$$

Inside the particles, the total field $\{\mathbf{E}_i, \mathbf{H}_i\}$ satisfies the classical system of Maxwell's equations

$$\text{rot}\mathbf{H}_i = jk\varepsilon_i\mathbf{E}_i; \quad \text{rot}\mathbf{E}_i = -jk\mathbf{H}_i; \quad \text{in } D_i. \quad (2)$$

The following boundary conditions are satisfied on the particle surface:

$$\begin{aligned} \mathbf{n}_i \times (\mathbf{E}_i(P) - \mathbf{E}_e(P) - \mathbf{E}_0(P)) = \\ -d_{\perp}\mathbf{n}_i \times \nabla\{\mathbf{n}_i \cdot (\mathbf{E}_i(P) - \mathbf{E}_e(P) - \mathbf{E}_0(P))\}, \\ \mathbf{n}_i(\mathbf{H}_i(P) - \mathbf{H}_e(P) - \mathbf{H}_0(P)) = \\ -j\omega d_{\parallel}\{\mathbf{n}_i \times [\mathbf{D}_i(P) - \mathbf{D}_e(P) - \mathbf{D}_0(P)]\} \times \mathbf{n}_i; \quad P \in \partial D_i. \end{aligned} \quad (3)$$

At infinity, the scattered field satisfies the Silver-Müller radiation conditions [25]

$$\lim_{r \rightarrow \infty} r(\sqrt{\varepsilon_e}\mathbf{E}_e \times \frac{\mathbf{r}}{r} - \mathbf{H}_e) = 0; \quad r = |\mathbf{M}|. \quad (4)$$

Here $\varepsilon_{e,i}$ are dielectric constants of the media in the corresponding areas, \mathbf{n}_i are unit external normals to the surfaces ∂D_i , respectively, with $\text{Im}\varepsilon_e = 0$, $\text{Im}\varepsilon_i \leq 0$, $k = \frac{\omega}{c}$, \mathbf{D} is displacement of the electric field.

The Feibelman parameters d_{\perp}, d_{\parallel} for a flat interface ($y = 0$) are formally defined as follows [10]:

$$d_{\perp}(\omega) = \frac{\int \rho(x, \omega) x dx}{\int \rho(x, \omega) dx}, \quad d_{\parallel}(\omega) = \frac{\int \partial_x J_y(x, \omega) x dx}{\int \partial_x J_y(x, \omega) dx},$$

where $\rho(x, \omega)$ is density of surface charges induced by an external field, and $J(x, \omega)$ is density of currents. It is assumed that at the metal-dielectric interface the normal component of the current of free charges is zeroed, therefore $d_{\parallel}(\omega) = 0$ [22]. $d_{\perp}(\omega)$ is a complex quantity, its real part corresponds to the center of mass of the electron cloud of induced charges, the imaginary part describes the Landau damping. For gold: $d_{\perp} \sim 1$ nm.

Assume that the boundary problem of diffraction (1)–(4) is solvable in a unique way. In the case of a homogeneous sphere, this was established in [26].

Discrete Sources Method

To solve the boundary problem of diffraction (1)–(4), we will use the Discrete Sources Method (DSM) [23,24], which is a rigorous numerical-analytical surface-oriented method. Within the DSM, the representation for the approximate solution in each of the regions $D_{1,2,e}$ is built up as a finite linear combination of fields of lower order multipoles distributed along the symmetry axis of the particle [23]. This representation meets the system of Maxwell’s equations everywhere outside discontinuities in the characteristics of the medium and satisfies the radiation conditions at infinity in an explicit analytical form. The corresponding DS amplitudes are determined from the boundary conditions specified at the interfaces of different media $\partial D_{1,2}$. DSM allows estimating the error of the resulting solution by calculating the discrepancy of fields on the surfaces of particles. The latter circumstance makes it possible to calculate the optical characteristics of fields in the gap between particles with a given accuracy.

Let us start by constructing an approximate solution to the boundary problem (1)–(4) for the case of P -polarization of an incident plane wave. It is in this case that the most noticeable PR arises [23]. The external excitation field in this case can be written as

$$\begin{aligned} \mathbf{E}_0 &= (\mathbf{e}_x \cos \theta_0 + \mathbf{e}_z \sin \theta_0)\chi(x, z); \\ \mathbf{H}_0 &= -\sqrt{\varepsilon_e}\mathbf{e}_y\chi(x, z), \end{aligned} \tag{5}$$

where $\chi(x, z) = \exp\{-jk_e(x \sin \theta_0 - z \cos \theta_0)\}$, $k_e = k\sqrt{\varepsilon_e}$, and $(\mathbf{e}_x, \mathbf{e}_y, \mathbf{e}_z)$ is Cartesian basis.

We will build up fields in the regions $D_{1,2,e}$ based on the vector potentials induced by sources distributed along the symmetry axis of the scatterer. The potentials can be written in the following form [23]:

$$\begin{aligned} \mathbf{A}_{mn}^{1,\alpha} &= Y_m^\alpha(\xi, z_n^\alpha)\{\mathbf{e}_\rho \cos[(m+1)\varphi] - \mathbf{e}_\varphi \sin[(m+1)\varphi]\}; \\ \alpha &= 1, 2, e; \\ \mathbf{A}_{mn}^{2,\alpha} &= Y_m^\alpha(\xi, z_n^\alpha)\{\mathbf{e}_\rho \sin[(m+1)\varphi] + \mathbf{e}_\varphi \cos[(m+1)\varphi]\}; \\ \mathbf{A}_n^{3,\alpha} &= Y_0^\alpha(\xi, z_n^\alpha)\mathbf{e}_z. \end{aligned}$$

Here the corresponding functions have the following form

$$\begin{aligned} Y_m^i(\xi, z_n^i) &= h_m^{(1)}(k_i R_{z_n^i})\left(\frac{\rho}{R_{z_n^i}}\right)^m, \\ Y_m^e(\xi, z_n^e) &= h_m^{(2)}(k_e R_{z_n^e})\left(\frac{\rho}{R_{z_n^e}}\right)^m, \end{aligned}$$

where $h_m^{(1,2)}$ are spherical Hankel functions, $k_{i,e} = k\sqrt{\varepsilon_{i,e}}$, $\xi = (\rho, z)$, $\rho^2 = x^2 + y^2$, $R_{z_n}^2 = \rho^2 + (z - z_n)^2$, $\{z_n^\alpha\}_{n=1}^{N_\alpha^m}$ are coordinates of discrete sources. A special feature of the DSM application for the case of analysis of paired particles is the representation of an approximate solution for internal fields [23]. Whereas the classical scheme of the method represents internal fields through

spherical Bessel functions [24], and $\{z_n^i\}$ are located inside D_i , in our case Hankel functions $h_m^{(1)}$ are used to represent them, and the sources are located outside D_i , in the complex plane passing through the origin and perpendicular to the axis of rotation. That is, the z_n^i coordinates are complex: $\text{Re}z_n^i = 0$, and $\text{Im}z_n^i$ are located symmetrically relative to the axis of rotation OZ [23], taking both positive and negative values (Fig. 1).

Taking into account the above, the field representations in the case of P polarization take on the following form:

$$\begin{aligned} \mathbf{E}_\alpha^N &= \sum_{m=0}^M \sum_{n=1}^{N_\alpha^m} \left\{ p_{mn}^\alpha \frac{j}{k\varepsilon_\alpha} \text{rotrot}\mathbf{A}_{mn}^{1,\alpha} + q_{mn}^\alpha \frac{j}{\varepsilon_\alpha} \text{rot}\mathbf{A}_{mn}^{2,\alpha} \right\} \\ &+ \sum_{n=1}^{N_\alpha^0} r_n^\alpha \frac{j}{k\varepsilon_\alpha} \text{rotrot}\mathbf{A}_n^{3,\alpha}; \\ \mathbf{H}_\alpha^N &= \frac{j}{k} \text{rot}\mathbf{E}_\alpha^N, \quad \alpha = i, e. \end{aligned} \tag{6}$$

It is easy to verify that constructed fields (6) satisfy all conditions of the diffraction boundary problem (1)–(4) with the exception of boundary conditions (3). These are exactly the boundary conditions, from which the unknown amplitudes of discrete sources $\mathbf{p}_m^N = \{p_{mn}^\alpha, q_{mn}^\alpha, r_n^\alpha\}$, $\alpha = i, e$ are determined directly.

Once the amplitudes of the discrete sources have been determined, the scattered field can be calculated using representation (6). An important characteristic that describes the scatterer’s response to external excitation is the scattered field radiation pattern. It is determined as [25]

$$\mathbf{E}_e(M)/|\mathbf{E}^0(M)| = \frac{\exp(-jk_e r)}{r} \mathbf{F}(\theta, \varphi) + O(r^{-2}), \quad r \rightarrow \omega.$$

Following the asymptotics of scattered field (6), θ, φ components of the radiation pattern for the P polarization take on the following form:

$$\begin{aligned} F_\theta^P(\theta, \varphi) &= j \sum_{m=0}^M (j \sin \theta)^m \cos(m+1)\varphi \sum_{n=1}^{N_e^m} \{p_{mn}^e \cos \theta + q_{mn}^e\} \\ &\times \exp\{jk_e z_n^e \cos \theta\} - j \sin \theta \sum_{n=1}^{N_e^0} r_n^e \exp\{jk_e z_n^e \cos \theta\}, \\ F_\varphi^P(\theta, \varphi) &= -j \sum_{m=0}^M (j \sin \theta)^m \sin(m+1)\varphi \\ &\times \sum_{n=1}^{N_e^m} \{p_{mn}^e + q_{mn}^e \cos \theta\} \exp\{jk_e z_n^e \cos \theta\}. \end{aligned} \tag{7}$$

Another important characteristic when studying the diffraction by nanoscale structures is the extinction cross-section; it is this parameter that shows how much energy the structure takes for the absorption and scattering from the field of

a plane wave. It should be noted that the extinction cross-section is a few orders of magnitude greater than the scattering cross-section. In relation to the diffraction problem under consideration, the extinction cross-section will be determined as follows:

$$\sigma_{\text{ext}}^P(\theta_0) = -\frac{4\pi}{k_e} \text{Im}F_{\theta}^P(\pi - \theta_0, \pi). \quad (8)$$

The extinction cross-section is measured in nm^2 . In addition, we will also analyze the behavior of the field gain (G) in the gap between particles in the region of wavelengths λ :

$$F(\lambda) = |\mathbf{E}_e^N + \mathbf{E}^0|^2 / |\mathbf{E}^0|^2. \quad (9)$$

This quantity is dimensionless.

Numerical results

Let us proceed to the discussion of the results of numerical modeling. The quantum parameters for the GNOR model for gold are taken from [16]:

$$\hbar\omega_p = 9.02 \text{ eV}, \quad \hbar\gamma = 0.071 \text{ eV}, \quad v_F = 1.39 \cdot 10^{12} \text{ } \mu\text{m/s},$$

$$D = 8.62 \cdot 10^8 \text{ } \mu\text{m}^2/\text{s}.$$

Particles that make up the pair will be considered as prolate spheroids, which are often encountered in applications [8]. Let us fix the equivolume diameter of each particle as $D = 15 \text{ nm}$ and vary the ratio of the axes of the spheroids $r = b/a$. We denote the gap between the particles as δ and assume that the particles are in water ($n_e = 1.33$). The refraction index of the gold shell was calculated taking into account the frequency dispersion of the material [27]. In turn, values of the Feibelman parameter d_{\perp} for gold were taken from experimental data [28].

Since the values of d_{\perp} significantly depend on the characteristics of the environment external to the metal, we used a correction of the values of d_{\perp} measured for the gold-air interface. The correction is based on the following ratio:

$$\varepsilon_i + 2\varepsilon_e - \frac{2}{R}(\varepsilon_i - \varepsilon_e)d_{\perp} = 0,$$

obtained in the case of PR for a sphere with a radius of R in [26]. From the latter relationship it follows that

$$d_{\perp} = 0.5R \frac{\varepsilon_i + 2\varepsilon_e}{\varepsilon_i - \varepsilon_e}. \quad (10)$$

Unfortunately, it is impossible to determine „numerical“ value of the parameter d_{\perp} from (10), because it depends on the radius of the sphere, however, it is possible to correct the experimentally obtained values of d_{\perp}^0 for the metal-air interface for the metal-dielectric case, for example for water. To do this, it is sufficient to write relationship (10) for two different media and exclude the radius of the sphere. The result is as follows:

$$d_{\perp} = d_{\perp}^0 \frac{\varepsilon_i + 2\varepsilon_e}{\varepsilon_i - \varepsilon_e} \frac{(\varepsilon_i - 1)}{\varepsilon_i + 2}. \quad (11)$$

Fig. 2 shows the results of solving the problem of diffraction of a plane wave by paired spheroids with the ratio of the axes $r = 2$ and the gap between them $\delta = 1 \text{ nm}$; the angle of incidence of the plane wave was taken equal to 90° . As it was established earlier in [23], at this angle of incidence the maximum PR amplitude is achieved. Fig. 2, *a* shows graphs of extinction cross-section (8) for the local case (LRA), bulk nonlocal case (GNOR), and the case of mesoscopic boundary conditions (SRF). As a result of tests for the precision of results in terms of residual error for the parameters corresponding to Fig. 2, *a*, we have succeeded in establishing the following. The relative residual error of the field in the mesh norm L_2 on the particle surface $\Delta \leq 0.5\%$ guarantees three correct digits of the extinction cross-section σ_{ext}^P for the cases of LRA and SRF. As for the GNOR case, the residual value $\Delta \sim 0.5\%$ guarantees an error of the results of the same order: $\Delta\sigma_{\text{ext}}^P \sim 0.5\%$. Moreover, in the results shown in Fig. 2, *a* the GNOR error was equal to unity of the third digit of the extinction cross-section. More detailed information about the relationship between the error in the results of solving the diffraction problems for nanoobjects with surface the residual value is given in [29].

Fig. 2, *b* shows results for the field enhancement factor (EF) in the gap (9) for a pair of spheroids with the same parameters. From the results shown in the figures, it is clear that, in comparison with the nonlocality bulk effect of GNOR, the use of mesoscopic boundary conditions leads to a significant restoration of the PR amplitude and a decrease in the shift toward the short-wavelength region. This is especially noticeable in the graphs of the field enhancement factor in the gap. It should be noted that the latter result is not unexpected, because the Feibelman parameter describes the surface effect of nonlocality, which plays a significant role when particles approach each other.

Fig. 3 shows the calculation results obtained for a fixed gap of $\delta = 1 \text{ nm}$ between particles with different axis ratios. In all cases, the equivolume diameter of each particle was constant, $D = 15 \text{ nm}$. Fig. 3, *a* shows the behavior of the extinction cross-section. It is obvious that as the elongation of the spheroids increases, the amplitude increases but the shift in the frequency domain changes insignificantly. The PR amplitude for the surface quantum effect turns out to be slightly smaller than that in the classical case, and the shift toward the short-wavelength region is less than 10 nm .

Fig. 3, *b* shows similar results for the gain. In this case, a change in the elongation of particles leads to a significant shift in the position of the PR in the wavelength region. For example, the position of the PR during deformation from $r = 2$ to $r = 4$ changes by 200 nm ! As before, the PR amplitude for SRF turns out to be smaller than that in the classical case, and the decrease ranges from 30% to 50%.

Fig. 4 shows the calculation results obtained for a fixed elongation of spheroids $r = 3$ and a varying gap between particles $\delta = 2, 1, 0.5 \text{ nm}$.

Fig. 4, *a* shows graphs of the extinction cross-section, and Fig. 4, *b* shows corresponding graphs of the enhancement

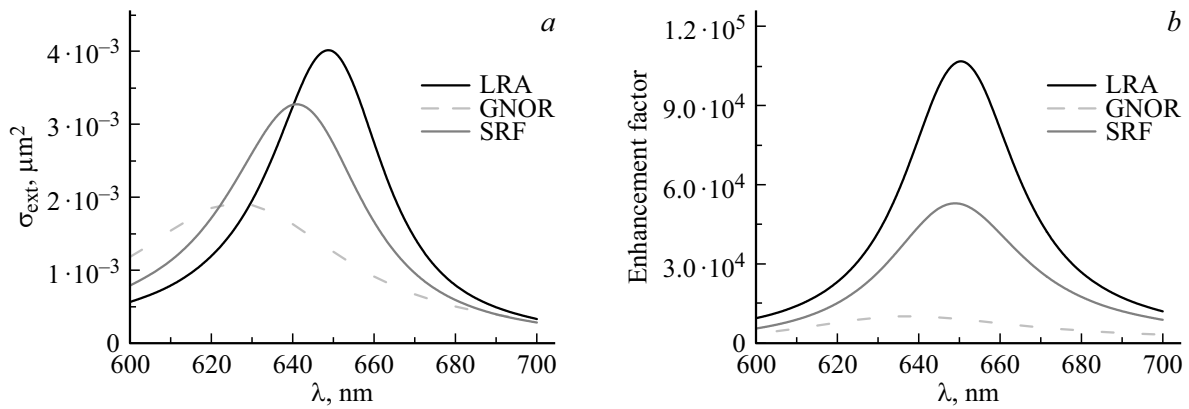


Figure 2. Comparison of local (LRA) and bulk nonlocal (GNOR) approaches with the case of mesoscopic boundary conditions (SRF) for a pair of spheroids with an axial ratio of $r = 2$ and a gap between them of $\delta = 1$ nm for the incidence of a plane wave at an angle of 90° : extinction cross-section (a), enhancement factor in the gap (b).

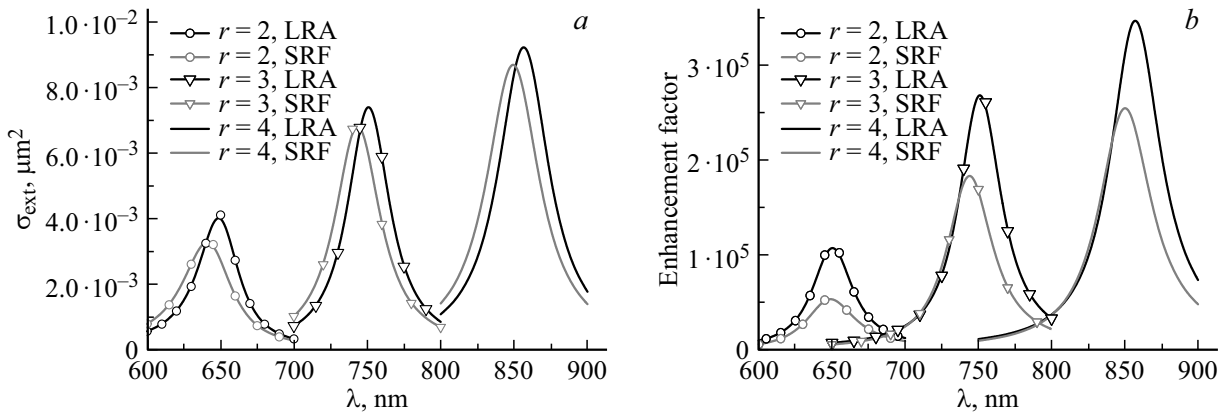


Figure 3. Calculations using mesoscopic boundary conditions (SRF) versus local case (LRA) for a pair of spheroids with different axis ratio: $r = 2, 3, 4$; gap is $\delta = 1$ nm; angle of incidence is $\theta_0 = 90^\circ$, equivolume diameter is $D = 15$ nm. Extinction cross-section (a), enhancement factor in the gap (b).

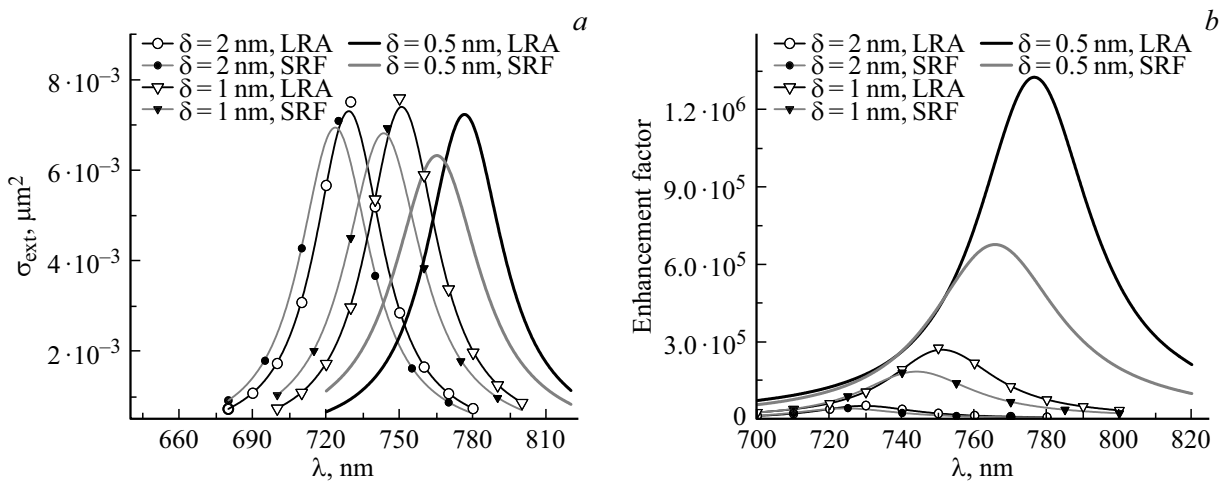


Figure 4. Comparison of results obtained using mesoscopic boundary conditions (SRF) and classical theory (LRA) for a pair of spheroids with different gaps between them: $\delta = 0.5, 1, 2$ nm; axis ratio is $r = 3$, angle of incidence is $\theta_0 = 90^\circ$, equivolume diameter is $D = 15$ nm. Extinction cross-section (a), enhancement factor in the gap (b).

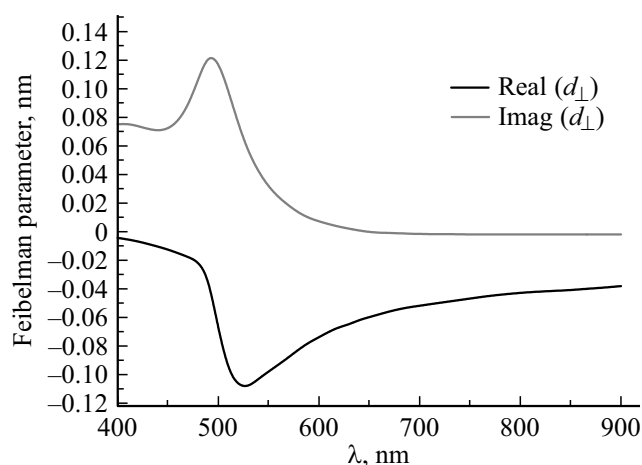


Figure 5. Experimentally measured real and imaginary parts of the Feibelman parameter d_{\perp} [28].

factor of intensity in the gap. It can be seen from Fig. 4, *a* that decrease in the gap results in a slight decrease in the PR values and its noticeable shift to the long-wavelength region of the spectrum. The PR amplitude for the SRF case decreases by no more than 15% compared to the classical case. More noticeable changes can be seen in Fig. 4, *b*, where similar curves for enhancement factor are shown. In this case, a decrease in the gap entails an increase in the PR by almost an order of magnitude with a shift to the long-wavelength region by almost 50 nm. At the same time, the decrease in the PR value for surface nonlocality can be as strong as 50% with a shift of the order of 10 nm.

After considering the results obtained, one general remark should be made. In noble metals (gold, silver), the splitting of the electron cloud near the surface occurs in such a way that its center is located inside the metal (the so-called *spill in*) (see Fig. 5) in contrast to metals of the alkali group (sodium), where the electron cloud leaks outward (*spill out*). This is why in the case of paired Na particles it is not possible to reliably describe the results for $\delta < 1.5$ nm [19]. In our case, the center of the electron cloud shifts inside the particles, because $\text{Re}d_{\perp} < 0$, which actually leads to „a decrease“ in particle size and, accordingly, to „an increase“ in the gap width δ . These circumstances entail a decrease in the PR amplitude and a shift to the short-wavelength region (*blue shift*) in the case of surface quantum effects.

Conclusion

The following main results were obtained in this study.

1. The Discrete Sources Method was adapted to the investigation of the influence of surface quantum effects described by mesoscopic boundary conditions with Feibelman parameters.

2. As a result of a comparative analysis of bulk and surface nonlocality, it was established that taking into account surface quantum effects leads to the restoration of

the PR amplitude. A similar situation has already been noted for isolated spheres in [30].

3. It is shown that the surface quantum effect, compared to the classical local case, leads to a decrease in the PR amplitude and a slight shift to the region of short wavelengths. This circumstance is a consequence of the effect of pressing the electron cloud, induced by an external field, into the particles, which corresponds to a decrease in the particle size and an increase in the gap size.

Funding

The study was carried out with financial support from the Ministry of Education and Science of the Russian Federation within the program of the Moscow Center for Fundamental and Applied Mathematics under agreement № 075-15-2022-284.

Conflict of interest

The authors declare that they have no conflict of interest.

References

- [1] M. Pelton, G. Bryant. *Introduction to Metal-Nanoparticle Plasmonics* (John Wiley & Sons, 2013). ISBN: 978-1-118-06040-7
- [2] *Modern Plasmonics (Handbook of Surface Science)*. Vol. 4, ed. by A.A. Maradudin, J.R. Sambles, W.L. Barnes (Elsevier, Amsterdam, 2014). ISBN 10: 0444595260
- [3] Y. Qiu, C. Kuang, X. Liu, L. Tang. *Sensors*, **22**, 4889 (2022). DOI: 10.3390/s22134889
- [4] H.-M. Kim, J.-H. Park, S.-K. Lee. *Spectrochimica Acta Part A: Molecular and Biomolecular Spectroscopy*, **261**, 120034 (2021). DOI: 10.1016/j.saa.2021.120034
- [5] M. Zhang, Y. Xu, X. Peng, H. Chen, H. Wang. *Chem. Commun.*, **58**, 7932 (2022). DOI: 10.1039/D2CC00801G
- [6] A.I. López-Lorente. *Analytica Chimica Acta*, **1168**, 338474 (2021). DOI: 10.1016/j.aca.2021.338474
- [7] H. Zhou, Q. Yu, H. Wang, W. Zhu, J. Liu, Z. Wang. *Talanta*, **233**, 122515 (2021). DOI: 10.1016/j.talanta.2021.122515
- [8] S. Farooq, D. Rativa, Z. Said, R.E. De Araujo. *Applied Thermal Engineering*, **218**, 119212 (2023). DOI: 10.1016/j.applthermaleng.2022.119212
- [9] H.M. Baghramyan, C. Ciraci. *Nanophotonics*, **11**—, (11), 2473 (2022). DOI: 10.1515/nanoph-2021-0707
- [10] N.A. Mortensen. *Nanophotonics*, **10** (10), 2563 (2021). DOI: 10.1515/nanoph-2021-0156
- [11] R. Esteban, A. Zugarramurdi, P. Zhang, P. Nordlander, F.J. García-Vidal, A.G. Borisov, J. Aizpurua. *Faraday Discussions*, **178**, 151 (2015). DOI: 10.1039/C4FD00196F
- [12] W. Zhu, R. Esteban, A.G. Borisov, J.J. Baumberg, P. Nordlander, H.J. Lezec, J. Aizpurua, K.B. Crozier. *Nature Commun.*, **7**, 11495 (2016). DOI: 10.1038/ncomms11495
- [13] C.A. Ullrich. *Time-Dependent Density-Functional Theory: Concepts and Applications* (OUP Oxford, 2011). ISBN-10: 0199563020
- [14] R. Sinha-Roy, P. García-González, H.-C. Weissker, F. Rabiloud, A.I. Fernández-Domínguez. *ACS Photonics*, **4**, 1484 (2017). DOI: 10.1021/acsp Photonics.7b00254

- [15] C. David, F.J. García de Abajo. *J. Phys. Chem. C*, **115**(40), 19470 (2011). DOI: 10.1021/jp204261u
- [16] N.A. Mortensen, S. Raza, M. Wubs, T. Søndergaard, S.I. Bozhevolnyi. *Nature Communications*, **5**, 3809 (2014). DOI: 10.1038/ncomms4809
- [17] M. Kupresak, X. Zheng, A.E. Vandenbosch, V.V. Moshchalkov. *Appl. Phys. Rev.*, **3**(1), 1900172 (2020). DOI: 10.1002/adts.201900172
- [18] H.M. Baghrmian, F. Della Sala, C. Cirací. *Phys. Rev. X*, **11**, 011049 (2021). DOI: 10.1103/PhysRevX.11.011049
- [19] A. Babaze, E. Ogando, P.E. Stamatopoulou, C. Tserkezis, N.A. Mortensen, J. Aizpurua, A.G. Borisov, R. Esteban. *Optics Express*, **30**—, (12), 21159 (2022). DOI: 10.1364/OE.456338
- [20] P.J. Feibelman. *Prog. Surf. Sci.*, **12**, 287 (1982). DOI: 10.1016/0079-6816(82)90001-6
- [21] Y. Yang, D. Zhu, W. Yan, A. Agarwal, M. Zheng, J.D. Joannopoulos, P. Lalanne, T. Christensen, K.K. Berggren, M. Soljačić. *Nature*, **576**, 248 (2019). DOI: 10.1038/s41586-019-1803-1
- [22] P.E. Stamatopoulou, C. Tserkezis. *Optical Materials Express*, **12**(5) 1869 (2022). DOI: 10.1364/OME.456407
- [23] N.V. Grishina, Yu.A. Eremin, A.G. Sveshnikov. *Opt. Spectrosc.*, **113**(4), 440 (2012). DOI: 10.1134/S0030400X12100049
- [24] Yu.A. Eremin, V.V. Lopushenko. *Opt. and spectrosc.*, **130**(10), 1596 (2022) (in Russian). DOI: 10.21883/OS.2022.10.53632.3849-22 [Yu.A. Eremin, V.V. Lopushenko. *Opt. Spectrosc.*, **130**(10), 1336 (2022). DOI: 10.21883/EOS.2022.10.54873.3849-22]
- [25] D. Colton, R. Kress. *Integral Equation Methods in Scattering Theory* (John Wiley & Son, New York, 1983).
- [26] P.A.D. Gonçalves, T. Christensen, N. Rivera, A.-P. Jauho, N.A. Mortensen, M. Soljačić. *Nat. Commun.*, **11**, 366 (2020). DOI: 10.1038/s41467-019-13820-z
- [27] P.B. Johnson, R.W. Christy. *Phys. Rev. B*, **6**, 4370 (1972). DOI: 10.1103/PhysRevB.6.4370
- [28] R.A. Echarri, P.A.D. Gonçalves, C. Tserkezis, F.J. García de Abajo, N.A. Mortensen, J.D. Cox. *Optica*, **8**(5), 710 (2021). DOI: 10.1364/OPTICA.412122
- [29] Yu.A. Eremin, N.L. Tsitsas, M. Kouroublakis, G. Fikioris. *J. Comput. Appl. Mathematics*, **417**, N114556 (2022). DOI: 10.1016/j.cam.2022.114556.
- [30] Q. Zhou, P. Zhang, X.-W. Chen. *Phys. Rev. B*, **105**, 125419 (2022). DOI: 10.1103/PhysRevB.105.125419

Translated by Ego Translating